Microscopic origin of pressure-induced phase transitions in the iron pnictide superconductors AFe_2As_2: An *ab initio* molecular dynamics study

Yu-Zhong Zhang, Hem C. Kandpal, Ingo Opahle, Harald O. Jeschke, and Roser Valentí
Institut für Theoretische Physik, Goethe-Universität Frankfurt, Max-von-Laue-Straße 1, 60438 Frankfurt am Main, Germany
(Received 29 July 2009; revised manuscript received 17 August 2009; published 30 September 2009)

Using *ab initio* molecular dynamics we investigate the electronic and lattice structure of AFe_2As_2 (A=Ca,Sr,Ba) under pressure. We find that the structural phase transition (orthorhombic to tetragonal symmetry) is always accompanied by a magnetic phase transition in all the compounds while the nature of the transitions is different for the three systems. Our calculations explain the origin of the existence of a collapsed tetragonal phase in $CaFe_2As_2$ and its absence in $BaFe_2As_2$. We argue that changes in the Fermi-surface nesting features dominate the phase transitions under pressure rather than spin frustration or a Kondo scenario. The consequences for superconductivity are discussed.

DOI: 10.1103/PhysRevB.80.094530 PACS number(s): 74.62.Fj, 74.70.−b, 61.50.Ks, 71.15.Pd

The discovery of iron pnictide superconductors[1] with critical temperatures T_c up to 57.4 K (Ref. 2) upon doping has strongly revived the interest in high-T_c superconductivity. The undoped Fe-based parent compound undergoes at low temperatures a structural transition from tetragonal to orthorhombic symmetry accompanied by a magnetic phase transition to a stripe-type spin-density-wave state.[3–7] While the nature of these two transitions is different between LaFeAsO (1111 compound) and AFe_2As_2 (122 compound) with A=(Ba,Sr,Ca), superconductivity appears in both material classes only when the lattice distortion and magnetic ordering are suppressed, indicating a strong competition between the structural distortion, magnetic ordering, and superconductivity in iron pnictides.

Recently, superconductivity in the parent compounds 1111 and 122 was reported under application of pressure.[8–25] In LaFeAsO,[8] resistivity measurements show superconductivity at $\approx$12 GPa with T_c=21 K. In $BaFe_2As_2$ superconductivity is found to appear gradually with increasing pressure while in $SrFe_2As_2$ the onset of superconductivity occurs abruptly.[22] In $CaFe_2As_2$,[12–14] detailed neutron- and x-ray diffraction analysis shows that the system undergoes a first-order phase transition from a magnetic orthorhombic to a nonmagnetic "collapsed" tetragonal phase under pressure. The possible appearance of superconductivity in this collapsed tetragonal phase is presently under debate.[15,16] While various experiments give different values of critical pressures[17–25] due to the fact that the phase transition is sensitive to possible nonhydrostatic pressure effects, Sn content in some samples, or the use of single crystals or polycrystalline material for structure determination, it is claimed that $BaFe_2As_2$ and $SrFe_2As_2$ do not manifest a collapsed tetragonal phase at elevated pressure.[13,17,18,23,24] Therefore, the fact that structurally similar compounds exhibit phase transitions of different nature urgently calls for a theoretical understanding. Moreover, it is still under intensive debate which is the driving mechanism of the collinear stripe-type antiferromagnetic ordering; whether the Fermi-surface nesting or the competition of exchange antiferromagnetic interactions between the nearest-neighbor and next-nearest-neighbor irons.[26–37]

Theoretical work on optimization of cell parameters and atomic positions under pressure within the framework of density-functional theory (DFT) has been done on AFe_2As_2 (A=Ca,Ba,Sr) (Refs. 38–40) and LaOFeAs.[38,41] However, by considering Vanderbilt-type ultrasoft pseudopotentials, Yildirim[38] obtained a smooth structural transition for $CaFe_2As_2$ under pressure, observing neither a sudden sizable increase in the cell parameters a and b nor a strong decrease in the cell parameter c which is inconsistent with experimental results.[12] Xie *et al.*[39] optimized within the full potential linearized augmented plane-wave method (FPLAPW) the orthorhombic lattice structure for $BaFe_2As_2$ under pressure by relaxing the internal parameter z_{As} and the c/a ratio while keeping the b/a ratio fixed. This procedure does not allow for the detection of the structural and magnetic phase transitions. Opahle *et al.*[41] investigated LaOFeAs under pressure and found that the system is close to a magnetic instability. Obviously, a complete and unambiguous theoretical description of the pressure-induced phase transitions in AFe_2As_2 (A=Ca,Sr,Ba) is still missing.

In this paper, we employ the Car-Parrinello[42] projector-augmented wave[43] molecular dynamics method at constant pressure[44] in order to investigate the pressure-induced phase transitions for AFe_2As_2 (A=Ca,Sr,Ba). Since in such transitions the interplay among electronic, magnetic, and lattice dynamics is essential, a combined *ab initio* DFT with molecular dynamics approach as used in the present work is very suitable. In such a procedure, at each pressure value a full, unbiased relaxation of all lattice and electronic degrees of freedom is performed in time steps of 0.12 fs at zero temperature. We used $4\times4\times4$ k points in doubled ($\sqrt{2}\times\sqrt{2}\times1$) unit cells. We used high energy cutoffs of 612 and 2448 eV for the wave functions and charge-density expansion, respectively. The total energy was converged to less than 0.01 meV/atom and the cell parameters to less than 0.0005 Å. The $3s3p3d$ ($4s4p4d/5s5p5d$) states in Ca (Sr/Ba) and the $3d4s4p$ states in Fe and As are treated as valence states. We checked our calculations with the FPLAPW method as implemented in the WIEN2K code.[45] Very good agreement is found between these two methods. The Perdew-Burke-Ernzerhof generalized gradient approximation (GGA) to DFT has been used.

Our findings can be summarized as follows: we show that $CaFe_2As_2$ undergoes a first-order phase transition to a col-

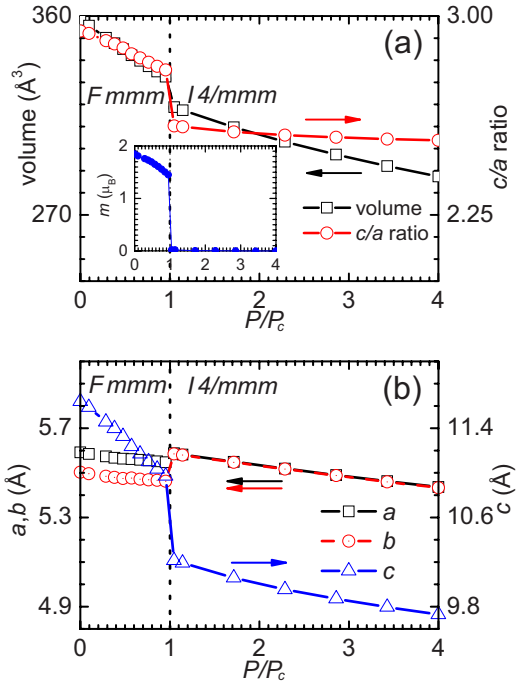

FIG. 1. (Color online) Calculated changes in (a) volume, c/a ratio, and magnetization (inset), (b) lattice parameters as a function of applied external pressure normalized to the critical pressure for $CaFe_2As_2$. The phase boundary between *Fmmm* and *I*4/*mmm* is indicated by the vertical dashed line.

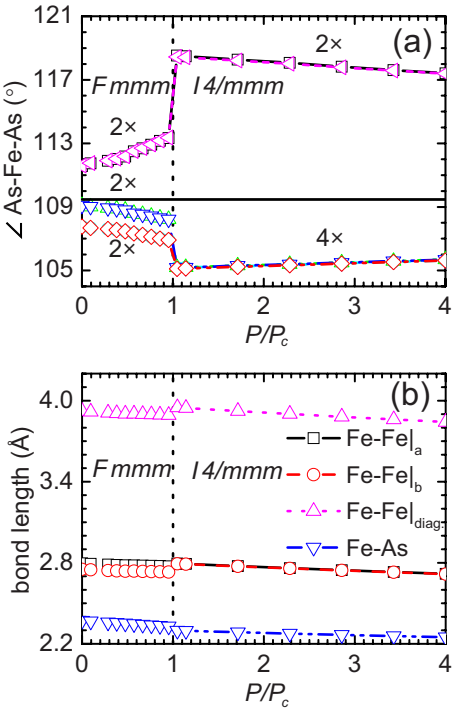

FIG. 2. (Color online) Calculated changes in (a) As-Fe-As angles and (b) Fe-Fe, Fe-As bond length as a function of applied external pressure normalized to the critical pressure for $CaFe_2As_2$. The phase boundary between *Fmmm* and *I*4/*mmm* is indicated by the vertical dashed line.

lapsed tetragonal phase with relative changes in lattice parameters, bond lengths, and angles agreeing very well with the experimental observations. In particular, our calculations can account for the measured expansion along the *ab* plane[12] at the critical pressure, which was not obtained in previous calculations. We also find an abrupt disappearance of magnetization at the critical pressure. For $SrFe_2As_2$ and $BaFe_2As_2$, where less is known about the details of the lattice structure and magnetization changes under pressure, we obtain a simultaneous structural (orthorhombic to tetragonal) and magnetic phase transition at high pressure. However, we observe a weak first-order phase transition for $SrFe_2As_2$ and a continuous phase transition for $BaFe_2As_2$ in contrast to the strongly first-order phase transition in $CaFe_2As_2$. We explain the microscopic origin of these differences in terms of the different Fermi-surface behavior under pressure. Finally, we argue that the existence of a magnetic transition from a striped AF state to a nonmagnetic state under pressure is mainly driven by changes in the Fermi-surface nesting rather than spin frustration or a Kondo scenario.[46]

In Figs. 1(a) and 1(b) we present the calculated changes in the volume and lattice parameters of $CaFe_2As_2$ as a function of pressure. The volume and the lattice parameter c decrease gradually with increasing pressure and show a discontinuous shrinkage at the critical pressure, where the system undergoes a structural phase transition from orthorhombic symmetry to a volume-collapsed tetragonal symmetry. Our results are in very good agreement with experimental data[12] with a volume collapse of $\Delta V^{\mathrm{th}} \approx 4.1\%$, $\Delta V^{\mathrm{exp}} \approx 4\%$. Moreover, the magnetization sharply goes to zero as shown in the inset of Fig. 1(a). Surprisingly, however, the lattice parameters a and b show abrupt expansions at the phase boundary although otherwise they show a monotonous compression in both phases. Such expansions, as also observed in experiments,[12] were not detected in previous DFT calculations and have a fundamental physical origin. In the orthorhombic phase below the critical pressure, the system shows collinear AF ordering within *ab* plane. At the critical pressure, the AF ordering is destroyed and the Pauli principle becomes more effective due to the appearance of more parallel Fe spins giving rise to a non-negligible lattice expansion along a and b.[47] As a consequence, the Fe-Fe bond length increases at the phase transition as observed in Fig. 2(b). In contrast, the As atoms move toward the Fe plane at the phase transition and the Fe-As bond length suddenly decreases with a relative shrinkage of $\Delta d^{\mathrm{th}}_{\mathrm{Fe\text{-}As}} \approx 1.3\%$ in very good agreement with $\Delta d^{\mathrm{exp}}_{\mathrm{Fe\text{-}As}} \approx 1.2\%$. Accordingly, the angles of the tetrahedra are suddenly shifted away from the ideal tetrahedral value of 109.47° at the phase transition while in the orthorhombic and in the high-temperature tetragonal phase they are much closer to the ideal value [Fig. 2(a)]. The strong distortion of the tetrahedron enhances the crystal-field splitting between $d_{x^2-y^2}$, d_{xz}, d_{yz}, and d_{z^2}, d_{xy} (orbitals given in the $x \| a$, $y \| b$, $z \| c$ local reference frame). This can be seen in the density of states (DOS) shown in Fig. 3(a) where the two peaks just below (of $d_{x^2-y^2}$, d_{xz}, and d_{yz} character) and above (of d_{z^2}, d_{xy} character) the Fermi level in the high-temperature ambient-pressure tetragonal phase (dashed line) are further separated in the high-pressure volume-collapsed tetragonal phase (solid line).

One aspect of the calculations to be considered is that the

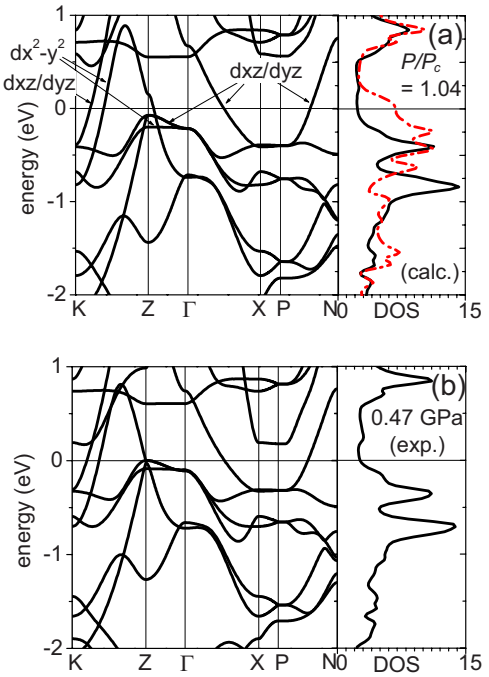

FIG. 3. (Color online) Comparison of the $CaFe_2As_2$ band structure and DOS in the collapsed tetragonal phase obtained from (a) our optimized lattice structure at $P/P_c=1.04$ and (b) the experimental lattice structure (Ref. 12) at $P^{\mathrm{exp}}/P_c^{\mathrm{exp}}\approx 1.6$. In (a) the total DOS for the high T tetragonal phase is also shown by the dashed line.

calculated critical pressure $P_c=5.25\pm0.25$ GPa is an order of magnitude larger than the experimental critical pressure $P_c^{\mathrm{exp}}\approx 0.3$ GPa. The overestimation of P_c in our calculations is a consequence of the well-known overestimation of volume and magnetic moment by GGA in the Fe pnictides at ambient pressure.[41,48] Therefore in order to reach the experimental structure conditions we have to go to higher simulation pressures. This procedure is proven to be valid since, as discussed above, we can reproduce the experimentally reported structural features of the phase transition in $CaFe_2As_2$, as well as the electronic properties in both orthorhombic phase[49] (not shown) and collapsed tetragonal phase as shown in Figs. 3(a) and 3(b) where we present the comparison between the electronic structure obtained from the Car-Parrinello-derived lattice structure (at $P/P_c=1.04$) and that obtained from the experimentally measured one (at 0.47 GPa, $P^{\mathrm{exp}}/P_c^{\mathrm{exp}}\approx 1.6$). We observe that the shapes of the total DOS are almost the same and only slight differences are found in details of the band structure. Therefore we can conclude that, although our calculations always overestimate the critical pressure, the phase transition and the physical properties in both phases can be quantitatively captured by our analysis.

In Figs. 4 and 5, we show the results for $SrFe_2As_2$ and $BaFe_2As_2$. We find that the structure and the magnetic phase transitions under pressure still occur simultaneously in these two compounds, but the nature of the phases is distinctly different from the $CaFe_2As_2$ case. $SrFe_2As_2$ shows smaller magnetization, volume, lattice and angles jumps at the critical pressure (see Fig. 4) compared to $CaFe_2As_2$ while we can hardly detect any discontinuity in $BaFe_2As_2$ (see Fig. 5). The simultaneous and abrupt change in the lattice structure and

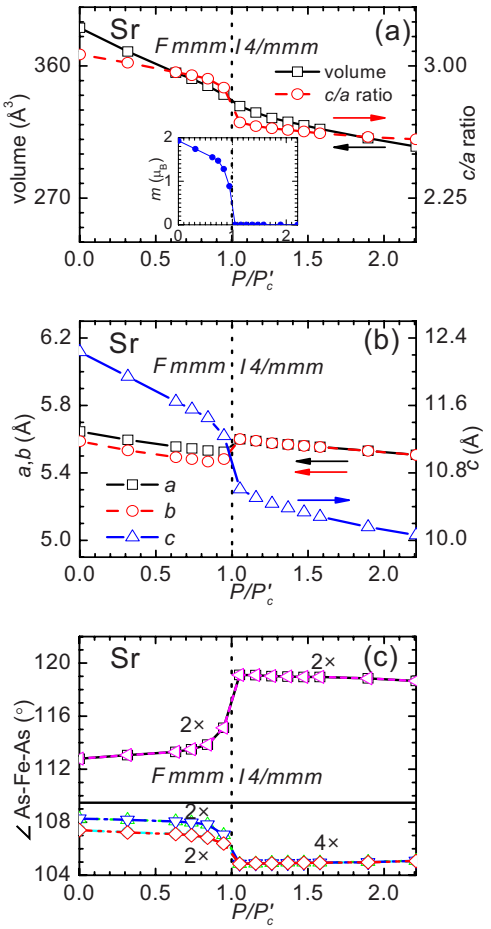

FIG. 4. (Color online) Calculated changes in (a) volume, c/a ratio, and magnetization (inset), (b) lattice parameters, and (c) As-Fe-As angles as a function of applied external pressure normalized to the critical pressure for $SrFe_2As_2$. The phase boundary between $Fmmm$ and $I4/mmm$ is indicated by the vertical dashed line.

the magnetization in $SrFe_2As_2$ is again consistent with recent experimental findings[17,18] while our results in $BaFe_2As_2$ have not yet been completely confirmed experimentally. Here, the pressure is again normalized to the critical simulated pressure $P_c'=9.5\pm0.5$ GPa for $SrFe_2As_2$ and $P_c''=17.5\pm0.5$ GPa for $BaFe_2As_2$. The calculated critical pressure for $SrFe_2As_2$ and $BaFe_2As_2$ is about 2–3 times larger than the experimental one while for $CaFe_2As_2$ it is around 20 times larger. This can be understood from the already mentioned overestimation of magnetic interactions and volumes in GGA calculations. Due to this, one would expect an (approximately constant) shift between the calculated and measured P_c, thus resulting in the large deviation for $CaFe_2As_2$ (where P_c is small) and the better agreement for $SrFe_2As_2$ and $BaFe_2As_2$.

In order to understand the microscopic origin of the differences in behavior between $SrFe_2As_2$, $BaFe_2As_2$, and $CaFe_2As_2$, we performed nonspin-polarized calculations with the optimized lattice structures and analyzed the band structures and Fermi surfaces. Below the critical pressure, we considered an average of lattice parameters a and b as a single lattice parameter in order to make the comparison of band structures of different phases (orthorhombic and tetrag-

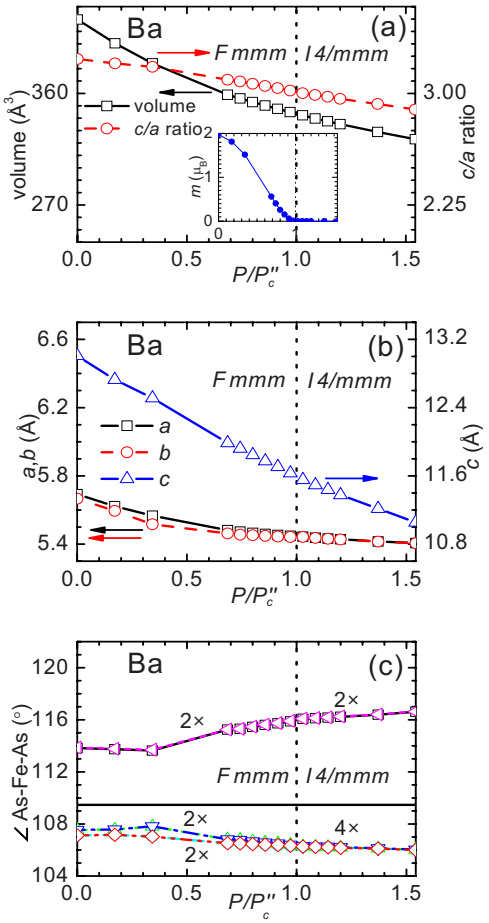

FIG. 5. (Color online) Calculated changes in (a) volume, c/a ratio, and magnetization (inset), (b) lattice parameters and (c) As-Fe-As angles as a function of applied external pressure normalized to the critical pressure for $BaFe_2As_2$. The phase boundary between *Fmmm* and *I*4/*mmm* is indicated by the vertical dashed line.

onal) possible within the same Brillouin zone. It has already been noticed that the tiny differences between a and b has no appreciable influence on the electronic structure.[41]

In Figs. 6 and 7 we show $k_z=0$, π/c, and $2\pi/c$ Fermi surface cuts of $CaFe_2As_2$ and $BaFe_2As_2$ at three different pressures. As a function of pressure, the changes in the Fermi surface in both compounds is remarkably different. Below P_c, $CaFe_2As_2$ shows with increasing pressure gradual shrinkages of the nested inner hole and electron cylinders around $(0,0,k_z)$ and $(\pi/a,\pi/a,k_z)$, respectively, leading to a reduction in the nesting features at each k_z (compare in Fig. 6 the rows at $P/P_c=0.1$ and $P/P_c=0.95$) and consequently a continuous reduction in the magnetization in the orthorhombic phase [inset of Fig. 1(a)]. As pressure increases to the critical region, the residual steep DOS at the Fermi level (Fig. 8) still forces the system to find a way to alleviate such an instability. However, the nested inner cylinders become too small to remove it by magnetic ordering. A sudden distortion of the tetrahedron is realized to lower the electronic energy by further splitting the Fe 3d orbitals [see the dashed DOS line in Fig. 3(a)] at the price of increasing the lattice energy. Thus, as shown in Fig. 6, $P/P_c=1.05$ row, right above the critical pressure all the cylinders around $(0,0,k_z)$ completely vanish

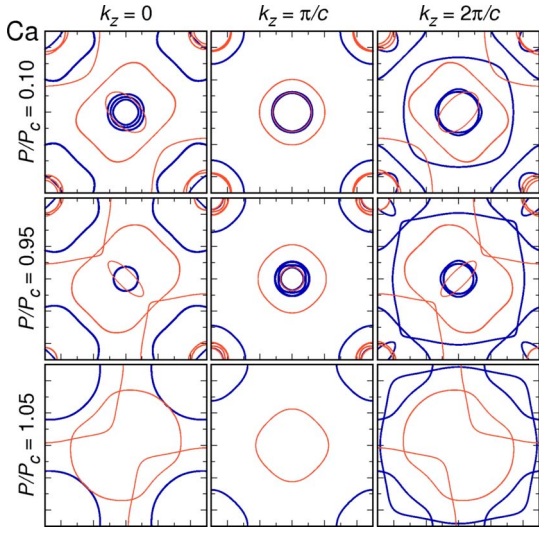

FIG. 6. (Color online) Fermi-surface cuts centered at $(0,0,k_z)$ with $k_z=0$, π/c, and $2\pi/c$ and $|k_x|$, $|k_y|\leq\pi/a$ at three pressure values for $CaFe_2As_2$. The Fermi-surface sheets are shown in black (blue). The gray (orange) sheets result from translating the sheets centered at $(\pi/a,\pi/a,k_z)$ by $(-\pi/a,-\pi/a,0)$ in order to see the nesting effects at $(0,0,k_z)$. Note, that the low P Fermi surface should not be compared to ambient P high-T Fermi surface as we always work at zero temperature. Here the pressures are normalized with respect to the critical pressure P_c for $CaFe_2As_2$.

due to the splitting of Fe 3d orbitals by lattice distortions in contrast to $BaFe_2As_2$ (see below) and accordingly, the magnetic ordering abruptly disappears [inset of Fig. 1(a)].

In contrast, the $BaFe_2As_2$ Fermi surface shows a shrinkage of the hole cylinders around $(0,0,k_z)$ into hole pockets while the Fermi-surface sheets around $(\pi/a,\pi/a,k_z)$ are changed insignificantly (see Fig. 7). Therefore, as the shrinkage occurs under pressure, the vanishing of Fermi-surface nesting at the lower k_z plane is partially compensated by the

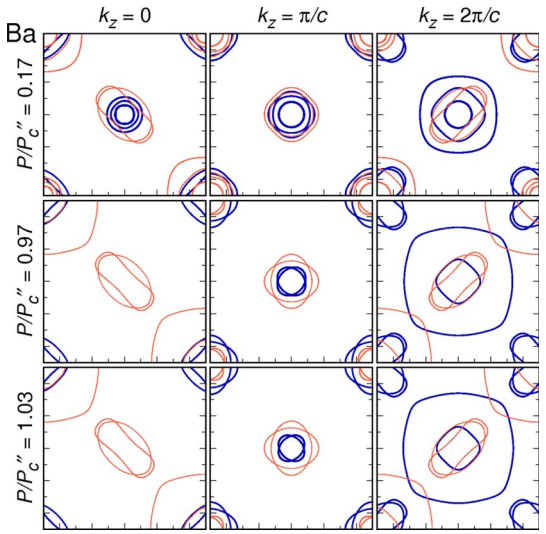

FIG. 7. (Color online) Fermi-surface cuts centered at $(0,0,k_z)$ with $k_z=0$, π/c, and $2\pi/c$ and $|k_x|$, $|k_y|\leq\pi/a$ at three pressure values for $BaFe_2As_2$. The color coding is the same as in Fig. 6. Here the pressures are normalized with respect to the critical pressure P_c'' for $BaFe_2As_2$.

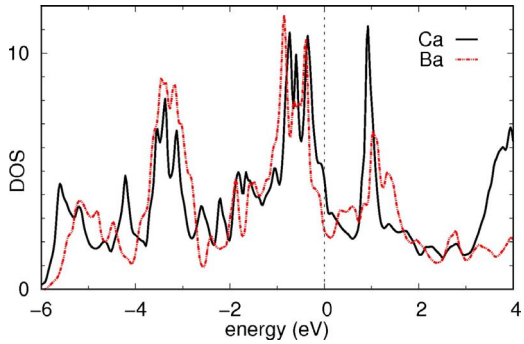

FIG. 8. (Color online) Total DOS for $CaFe_2As_2$ (continuous line) and $BaFe_2As_2$ (dashed line) at the critical pressure region.

appearance of new nestings at a higher k_z plane (e.g., Fig. 7 at $P/P_c''=0.17$ and $P/P_c''=0.97$), which prohibits the sudden change in magnetization since the nesting remains significant below the critical pressure (e.g., Fig. 7 at $k_z=2\pi/c$ and $P/P_c''=0.97$). Since lowering the total energy by magnetic ordering always prevails over abrupt lattice distortions, the sudden jump of the angles is suppressed as shown in Fig. 5(c). The slow change in the Fermi-surface topology as shown in Fig. 7 is consistent with the continuous reduction in magnetization as observed in the inset of Fig. 5(a).

Figure 9 presents the calculated noninteracting susceptibility $\chi_0(q)$ at $q=(\pi,\pi,0)$ as a function of pressure within the constant matrix element approximation[13,28,29,36] for all the three 122 compounds. The relation between the change in the Fermi-surface nesting features at $q=(\pi,\pi,0)$ and the phase transitions under pressure is clearly quantified with this magnitude. $\chi_0(q)$ at $q=(\pi,\pi,0)$ is the response for the observed Fermi-surface nesting-induced stripe-type antiferromagnetic ordering and while it shows a continuous decrease at elevated pressures in $BaFe_2As_2$, abrupt reductions at the phase transition are detected in both $CaFe_2As_2$ and $SrFe_2As_2$, indicating that the phase transition for these two systems are of first order where a sudden disappearance of the Fermi-surface nesting occurs. Moreover, we observe that the volume and lattice parameter discontinuities [Figs. 4(a) and 4(b)] and the tetrahedron distortion [Fig. 4(c)] right above the phase transition for $SrFe_2As_2$ are of the same nature as in $CaFe_2As_2$ but less pronounced. We conclude that the phase transition is of weak first order in $SrFe_2As_2$.

Finally, we find that the ground-state energy of the stripe-ordered AF state is always far below that of the checkerboard-ordered one in the orthorhombic phase while that of the high-pressure tetragonal phase is nonmagnetic, indicating that the phase transition under pressure for the three compounds is not driven by the competition between different magnetic ordering, i.e., spin frustration. Furthermore, the tiny crystal-field splittings of the Fe 3*d* states and strong itinerancy of all Fe 3*d* electrons does not support the Kondo scenario[46] for the phase transitions under pressure.

In conclusion, we investigated the phase transitions in the iron pnictide 122 compounds under pressure within the framework of *ab initio* molecular dynamics. The results on $CaFe_2As_2$ agree very well with the experimental findings. We show that magnetic and structural phase transitions also appear concomitantly in $SrFe_2As_2$ and $BaFe_2As_2$. While they

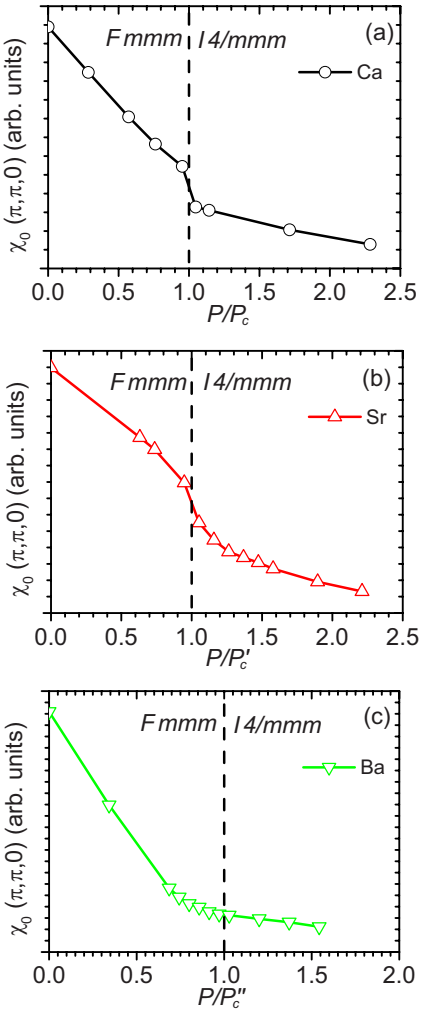

FIG. 9. (Color online) Calculated noninteracting susceptibility $\chi_0(q)$ at $q=(\pi,\pi,0)$ within the constant matrix element approximation as a function of the normalized pressure with respect to the critical one (in arbitrary units). This magnitude measures the response for the observed stripe-type antiferromagnetic ordering. The three panels correspond to: (a) $CaFe_2As_2$, (b) $SrFe_2As_2$, and (c) $BaFe_2As_2$. The phase boundary between *Fmmm* and *I*4/*mmm* symmetries is indicated by the vertical dashed line.

are weakly first order in $SrFe_2As_2$, the phase transition is continuous in $BaFe_2As_2$ which may be closely related to the different behavior of entering superconductivity between $SrFe_2As_2$ and $BaFe_2As_2$ observed experimentally.[22] The remaining hole pocket as well as nesting features in $BaFe_2As_2$ may be related to the highest transition temperature[22] observed among 122 compounds due to the remaining spin fluctuations. Since the topology of the Fermi surface in the high pressure phase is quite different among these 122 compounds and LaOFeAs,[41] the pairing mechanism may differ among these compounds although they belong to the same family of superconductors.

We thank Claudius Gros for discussions and the Deutsche Forschungsgemeinschaft for financial support through the SFB/TRR 49 and Emmy Noether programs and we acknowledge support by the Frankfurt Center for Scientific Computing.

[1] Y. Kamihara, T. Watanabe, M. Hirano, and H. Hosono, J. Am. Chem. Soc. **130**, 3296 (2008).
[2] P. Cheng, B. Shen, G. Mu, X. Zhu, F. Han, B. Zeng, and H. H. Wen, EPL **85**, 67003 (2009).
[3] C. de la Cruz, Q. Huang, J. W. Lynn, Jiying Li, W. Ratcliff II, J. L. Zarestky, H. A. Mook, G. F. Chen, J. L. Luo, N. L. Wang, and Pengcheng Dai, Nature (London) **453**, 899 (2008).
[4] Q. Huang, Y. Qiu, Wei Bao, M. A. Green, J. W. Lynn, Y. C. Gasparovic, T. Wu, G. Wu, and X. H. Chen, Phys. Rev. Lett. **101**, 257003 (2008).
[5] M. Rotter, M. Tegel, D. Johrendt, I. Schellenberg, W. Hermes, and R. Pöttgen, Phys. Rev. B **78**, 020503(R) (2008).
[6] A. I. Goldman, D. N. Argyriou, B. Ouladdiaf, T. Chatterji, A. Kreyssig, S. Nandi, N. Ni, S. L. Bud'ko, P. C. Canfield, and R. J. McQueeney, Phys. Rev. B **78**, 100506(R) (2008).
[7] J. Zhao, W. Ratcliff, J. W. Lynn, G. F. Chen, J. L. Luo, N. L. Wang, J. Hu, and P. Dai, Phys. Rev. B **78**, 140504(R) (2008).
[8] H. Okada, K. Igawa, H. Takahashi, Y. Kamihara, M. Hirano, H. Hosono, K. Matsubayashi, and Y. Uwatoko, J. Phys. Soc. Jpn. **77**, 113712 (2008).
[9] K. Igawa, H. Okada, H. Takahashi, S. Matsuishi, Y. Kamihara, M. Hirano, H. Hosono, K. Matsubayashi, and Y. Uwatoko, J. Phys. Soc. Jpn. **78**, 025001 (2009).
[10] T. Park, E. Park, H. Lee, T. Klimczuk, E. D. Bauer, F. Ronning, and J. D. Thompson, J. Phys.: Condens. Matter **20**, 322204 (2008).
[11] M. S. Torikachvili, S. L. Bud'ko, N. Ni, and P. C. Canfield, Phys. Rev. Lett. **101**, 057006 (2008).
[12] A. Kreyssig, M. A. Green, Y. Lee, G. D. Samolyuk, P. Zajdel, J. W. Lynn, S. L. Bud'ko, M. S. Torikachvili, N. Ni, S. Nandi, J. B. Leão, S. J. Poulton, D. N. Argyriou, B. N. Harmon, R. J. McQueeney, P. C. Canfield, and A. I. Goldman, Phys. Rev. B **78**, 184517 (2008).
[13] A. I. Goldman, A. Kreyssig, K. Prokes, D. K. Pratt, D. N. Argyriou, J. W. Lynn, S. Nandi, S. A. J. Kimber, Y. Chen, Y. B. Lee, G. Samolyuk, J. B. Leão, S. J. Poulton, S. L. Bud'ko, N. Ni, P. C. Canfield, B. N. Harmon, and R. J. McQueeney, Phys. Rev. B **79**, 024513 (2009).
[14] D. K. Pratt, Y. Zhao, S. A. J. Kimber, A. Hiess, D. N. Argyriou, C. Broholm, A. Kreyssig, S. Nandi, S. L. Bud'ko, N. Ni, P. C. Canfield, R. J. McQueeney, and A. I. Goldman, Phys. Rev. B **79**, 060510(R) (2009).
[15] W. Yu, A. A. Aczel, T. J. Williams, S. L. Bud'ko, N. Ni, P. C. Canfield, and G. M. Luke, Phys. Rev. B **79**, 020511(R) (2009).
[16] H. Lee, E. Park, T. Park, V. A. Sidorov, F. Ronning, E. D. Bauer, and J. D. Thompson, Phys. Rev. B **80**, 024519 (2009).
[17] M. Kumar, M. Nicklas, A. Jesche, N. Caroca-Canales, M. Schmitt, M. Hanfland, D. Kasinathan, U. Schwarz, H. Rosner, and C. Geibel, Phys. Rev. B **78**, 184516 (2008).
[18] H. Kotegawa, H. Sugawara, and H. Tou, J. Phys. Soc. Jpn. **78**, 013709 (2008).
[19] H. Kotegawa, T. Kawazoe, H. Sugawara, K. Murata, and H. Tou, J. Phys. Soc. Jpn. **78**, 083702 (2009).
[20] M. S. Torikachvili, S. L. Bud'ko, N. Ni, and P. C. Canfield, Phys. Rev. B **78**, 104527 (2008).
[21] H. Fukazawa, N. Takeshita, T. Yamazaki, K. Kondo, K. Hirayama, Y. Kohori, K. Miyazawa, H. Kito, H. Eisaki, and A. Iyo, J. Phys. Soc. Jpn. **77**, 105004 (2008).
[22] P. L. Alireza, Y. T. C. Ko, J. Gillett, C. M. Petrone, J. M. Cole, G. G. Lonzarich, and S. E. Sebastian, J. Phys.: Condens. Matter **21**, 012208 (2009).
[23] S. A. J. Kimber, A. Kreyssig, Y.-Z. Zhang, H. O. Jeschke, R. Valentí, F. Yokaichiya, E. Colombier, J. Yan, T. C. Hansen, T. Chatterji, R. J. McQueeney, P. C. Canfield, A. I. Goldman, and D. N. Argyriou, Nature Mater. **8**, 471 (2009).
[24] E. Colombier, S. L. Bud'ko, N. Ni, and P. C. Canfield, Phys. Rev. B **79**, 224518 (2009).
[25] A. Mani, N. Ghosh, S. Paulraj, A. Bharathi, and C. S. Sundar, EPL **87**, 17004 (2009).
[26] D. J. Singh and M.-H. Du, Phys. Rev. Lett. **100**, 237003 (2008).
[27] C. Fang, H. Yao, W.-F. Tsai, J. P. Hu, and S. A. Kivelson, Phys. Rev. B **77**, 224509 (2008).
[28] J. Dong, H. J. Zhang, G. Xu, Z. Li, G. Li, W. Z. Hu, D. Wu, G. F. Chen, X. Dai, J. L. Luo, Z. Fang, and N. L. Wang, EPL **83**, 27006 (2008).
[29] I. I. Mazin, D. J. Singh, M. D. Johannes, and M. H. Du, Phys. Rev. Lett. **101**, 057003 (2008).
[30] T. Yildirim, Phys. Rev. Lett. **101**, 057010 (2008).
[31] Q. Si and E. Abrahams, Phys. Rev. Lett. **101**, 076401 (2008).
[32] F. Ma, Z.-Y. Lu, and T. Xiang, Phys. Rev. B **78**, 224517 (2008).
[33] M. J. Han, Q. Yin, W. E. Pickett, and S. Y. Savrasov, Phys. Rev. Lett. **102**, 107003 (2009).
[34] F. Ma, W. Ji, J. Hu, Z.-Y. Lu, and T. Xiang, Phys. Rev. Lett. **102**, 177003 (2009).
[35] F. Ma, Z.-Y. Lu, and T. Xiang, arXiv:0806.3526 (unpublished).
[36] M. J. Han and S. Y. Savrasov, Phys. Rev. Lett. **103**, 067001 (2009).
[37] J. Zhao, D. T. Adroja, D.-X. Yao, R. Bewley, S. Li, X. F. Wang, G. Wu, X. H. Chen, J. Hu, and P. Dai, Nat. Phys. **5**, 555 (2009).
[38] T. Yildirim, Phys. Rev. Lett. **102**, 037003 (2009).
[39] W. Xie, M. Bao, Z. Zhao, and B. G. Liu, Phys. Rev. B **79**, 115128 (2009).
[40] Deepa Kasinathan, Alim Ormeci, Katrin Koch, Ulrich Burkhardt, Walter Schnelle, Andreas Leithe-Jasper, and Helge Rosner, New J. Phys. **11**, 025023 (2009).
[41] I. Opahle, H. C. Kandpal, Y. Zhang, C. Gros, and R. Valentí, Phys. Rev. B **79**, 024509 (2009).
[42] R. Car and M. Parrinello, Phys. Rev. Lett. **55**, 2471 (1985).
[43] P. E. Blöchl, Phys. Rev. B **50**, 17953 (1994).
[44] M. Parrinello and A. Rahman, Phys. Rev. Lett. **45**, 1196 (1980).
[45] P. Blaha, K. Schwarz, G. Madsen, D. Kvaniscka, and J. Luitz, in *WIEN2K, An Augmented Plane Wave+ Local Orbitals Program for Calculating Crystal*, edited by K. Schwarz (Technical University, Vienna, Austria, 2001).
[46] A. Hackl and M. Vojta, New J. Phys. **11**, 055064 (2009).
[47] Y.-Z. Zhang, H. O. Jeschke, and R. Valentí, Phys. Rev. Lett. **101**, 136406 (2008).
[48] I. I. Mazin, M. D. Johannes, L. Boeri, K. Koepernik, and D. J. Singh, Phys. Rev. B **78**, 085104 (2008).
[49] Y.-Z. Zhang, I. Opahle, H. O. Jeschke, and R. Valentí (unpublished).